NASA Technical Memorandum 89093

ELASTIC-PLASTIC STRESS CONCENTRATIONS AROUND CRACK-LIKE NOTCHES IN CONTINUOUS FIBER REINFORCED METAL MATRIX COMPOSITES

W. S. Johnson and C. A. Bigelow

February 1987

NASA
National Aeronautics and
Space Administration

Langley Research Center
Hampton, Virginia 23665

SUMMARY

Continuous fiber silicon-carbide/aluminum composite laminates with slits were tested statically to failure. Five different layups were examined: $[0]_8$, $[0_2/\pm45]_s$, $[0/90]_{2s}$, $[0/\pm45/90]_s$, and $[\pm45]_{2s}$. Either a 9.5 or a 19 mm slit was machined in the center of each specimen. The strain distribution ahead of the slit tip was found experimentally with a series of strain gages bonded ahead of the slit tip. A three-dimensional finite element program (PAFAC) was used to predict the strain distribution ahead of the slit tip for several layups. For all layups, except the $[0]_8$, the yielding of the metal matrix caused the fiber stress concentration factor to increase with increasing load. This is contrary to the behavior seen in homogeneous materials where yielding causes the stress concentration to drop. For the $[0]_8$ laminate, yielding of the matrix caused a decrease in the fiber stress concentration. The finite element analysis predicted these trends correctly.

I. INTRODUCTION

Metal matrix composites (MMC) are being considered for many applications in advanced aerospace structures primarily because of their superior dimensional stability and high temperature capability characteristics compared to resin matrix composites. In addition, continuous fiber-reinforced MMC offer very high stiffness-to-weight and strength-to-weight ratios when compared to monolithic metals. Most of the projected aerospace applications will be required to be damage tolerant. In order to perform a damage tolerance analysis, it is important that the stress state around notches be well defined. In continuous fiber-reinforced MMC, the matrix can yield while the fiber remains almost perfectly elastic. This combination of constituent properties can lead to stress concentrations at slit tips that are different than for elastic or elastic-plastic homogeneous materials. The implications of the matrix yielding have not been widely recognized or understood in the materials community. The purpose of this paper is to examine experimentally and analytically the matrix plasticity effect around slits, in particular, the effect on fiber stress concentrations.

Johnson, Bigelow, and Bahei-El-Din [1], and Poe and Sova [2] conducted a number of fracture tests on boron/aluminum (B/Al) laminates containing slits. Fiber and matrix damage was monitored by using radiography. Johnson, Bigelow, and Bahei-El-Din [1] found that first damage could be predicted by analytically monitoring the stress state in the boron fibers adjacent to the slit. When the fiber stress reached a predetermined value, damage occurred. First fiber failure occurred at approximately one half of the specimen's ultimate

strength for the slit unidirectional specimens. The first fiber failure in specimens with slits for $[\pm 45]_{2s}$, $[0/\pm 45]_s$, and $[0_2/\pm 45]_s$ laminate orientations occurred at or very near the specimens ultimate strength. Since the damage does not usually propagate in a self similar manner in aluminum MMC, traditional fracture mechanic quantities such as stress-intensity factors may be questionable for general application to laminated metal matrix composites. Failure predictions using the stress (or strain) state in the load carrying fibers just ahead of the slit may be the most viable approach for assessing damage tolerance [1-3].

This paper will present experimental data for silicon-carbide/ aluminum composites in a number of different layups. The strain state ahead of the slit tip was determined experimentally with small strain gages. The strain distribution ahead of the slit will be presented for load levels that result in material responses ranging from elastic to highly elastic-plastic. The stress-strain state will also be predicted analytically using a three-dimensional finite element program. The predictions will be compared to the experimental data to assess the suitability of the analysis model.

II. EXPERIMENTS

A. Specimens, Materials, and Preparations

Continuous fiber silicon-carbide/aluminum composite laminates with silts were tested statically to failure. The composite matrix material was 6061 aluminum which was annealed prior to testing. The fibers were 0.14-mm diameter silicon-carbide with a surface coating suitable for aluminum matrix applications. The fiber, designated

SCS_2, and the composite were manufactured by AVCO Specialty Materials Division, Lowell, MA, in the form of 450 by 450 mm plates.* Several of the supplied composite plates were slightly bowed. This resulted in some of the specimens being slightly curved. This problem will be addressed later in the text. The supplied laminates contained fibers that had lower moduli than suggested by the manufacturer as explained in reference [4]. The composite constituent properties are given in Table I while the laminate elastic moduli are given in Table II.

Five different layups were examined: $[0]_8$, $[0_2/\pm45]_s$, $[0/90]_{2s}$, $[0/\pm45/90]_s$, and $[\pm45]_{2s}$. Each specimen was 1.6 mm thick and was cut into a 51 by 164 mm rectangle using a diamond wheel saw. Either a 9.5 or 19 mm long center slit was electronically discharged machined (EDM) into each specimen. The slits were approximately 0.3 mm wide.

B. Experimental Procedures

A row of five small strain gages (each approximately 1 mm square) was bonded just ahead of the slit tip on one side of the specimen to measure axial strain. The strain gages were spaced 2.0 mm apart, centerline to centerline, as shown in Figure 1.

The specimens were loaded in a tensile displacement control mode using a servo-hydraulic test machine. Approximately 39 mm on each end of the specimen was used for gripping. A computer was used to record the strain versus load data for each strain gage. The specimens were loaded at approximately 0.5 mm per minute until they failed.

* Trades names are used to adequately describe the materials used and their use does not imply an endorsement by the National Aeronautics and Space Administration.

C. Results and Discussions

The failure stresses of the slit specimens are given in Table II. The strain gage results are shown in Figures 2 through 6. Each figure shows the data for both the 9.5 and the 19.0 mm slit lengths in a given laminate. The normalized strain distribution ahead of the slit tip is given for a low load level and a high load level. The strain distribution at the low load level is considered to be almost entirely elastic, while the higher stress level causes extensive yielding in the matrix material. The measured strains are normalized by the calculated remote elastic strain for each given load level. The calculated remote elastic strain at a given load was found by dividing the applied stress by the calculated longitudinal modulus of the laminate given in Table II. The actual remote strain may be nonlinear at the higher load levels and would, therefore, be greater than the calculated remote elastic strain.

As mentioned earlier, some of the test specimens had a slight curvature in the longitudinal direction. Therefore, upon tensile loading, some bending stresses were introduced. In order to compensate for this bending effect, the strain distributions were shifted such that the average value of the normalized strain for the elastic stress level was 1.6 for the 19-mm slit and 1.23 for the 9.5-mm slit. The values 1.6 and 1.23 are the ratios of the gross cross-sectional area to the net cross-sectional area for the respective slit lengths. For equilibrium, the same load must pass through both the net and gross sections. Thus, the average elastic strain in the net section will be higher than the remote strain, by the factor of the ratio of the gross area to the net area.

The strain concentrations just ahead of the slit tip (at 0.5 mm) are higher for the plastic strain distribution than for the elastic. Even if the strain data curves were to be shifted vertically such that they came together at 8.5 mm from the slit tip, the plastic strain concentration would still be higher than the elastic. The only exception is the $[0]_8$ laminate. Unidirectional laminates develop long, narrow plastic zones at the slit tip due to the intense shear stresses. These zones are parallel to the fibers as noted by Jones and Goree [5] and shown in Figure 7. This shear yielding greatly reduces the strain concentration ahead of the slit. Therefore, in Figure 6, the strain distribution for the $[0]_8$ is rather flat for the high load, plastic case and the slit-tip strain concentration is lower for the plastic case than for the elastic case.

For all laminates containing 0^o plies, the axial strain measured at a point on the surface should be a good indicator of the stress in the 0^o fibers beneath. The experimental data clearly indicate that the yielding of the matrix material causes the strain concentration near the slit tip to rise for all layups examined except the unidirectional case. Therefore, for all layups except the unidirectional, the axial stresses in the 0^o fibers just ahead of the slit are significantly higher due to the plastic deformation of the matrix material than would be predicted with an elastic analysis. The analytical prediction capabilities will be examined in the next section.

III. ANALYSIS

A. Homogeneous Materials

In homogeneous metallic materials such as aluminum alloys, yielding reduces the slit-tip stress concentration, as illustrated in Figure 8. Here the stress distribution ahead of the slit, calculated using a finite element program, is shown for a center cracked, aluminum specimen. The specimen is 19.26 mm wide, 84.07 mm long, with a slit of length 5.49 mm located in the center of the specimen. The aluminum material is modeled using the same properties as the matrix material in the composite laminates. Predictions based on a stress failure criteria, using the elastic response, would be conservative for a specimen that had experienced yielding. However, this is not, in general, the case for metal matrix composites. As was shown by the experimental results of the previous section, yielding causes the slit-tip strain concentration to increase. This will be confirmed analytically in the following section.

B. Metal Matrix Composites

In metal matrix composites, the matrix yields, whereas the fibers generally behave elastically until they break. Therefore, to model the behavior of metal matrix composites, the elastic-plastic behavior of the matrix and the elastic behavior of the fiber must be accounted for.

1. Finite element analysis

An analysis that models this two phase behavior was used in the present study. This analysis was conducted with a three-dimensional

finite element program [6] called PAFAC (Plastic And Failure Analysis of Composites), which was developed from a program written by Bahei-El-Din et al. [7,8]. PAFAC uses a constant strain, eight-noded, hexahedral element. Each hexahedral element represents a unidirectional composite material whose fibers can be oriented in the appropriate direction in the structural (Cartesian) coordinate system.

Material model. - The PAFAC program uses a continuum material model developed by Bahei-El-Din and Dvorak [8,9,10] to represent the essential aspects of the elastic-plastic behavior of composite laminates. The material model is briefly described in the Appendix.

Description of meshes. - Previous analyses using PAFAC [1,6] used a radial mesh, such as shown in Figure 9(a). However, at the time of the previous analysis [1,6] the authors felt that a high shear zone did not exist for slit laminates containing both 0^{o} and angle plies. Recently, Post et al. [11] found rather significant shear zones at a slit tip in a $[0/\pm45]_{s}$ layup of boron/aluminum. Figure 10 shows a typical Moire fringe pattern found by Post et al. which illustrates the high shear band at the slit tip. It was felt that a radial mesh would not adequately model these high shear zones typically seen in front of the slit tip in 0^{o} layers. Thus, a rectangular mesh, with a rectangular slit tip, as shown in Figure 9(b), was also used in the present work to determine the effects of mesh type. Both meshes shown in Figure 9 have the same size element at the crack tip. The crack tip element was sized to represent one fiber spacing (0.178 mm).

2. Comparison of experimental and analytical results

Figure 11 compares the predictions using the rectangular and radial meshes with the experimental results for the $[0]_8$ laminate with 2a = 19 mm. As before, these results are presented as normalized strains ahead of the slit tip. The solid and dashed curves show the predictions using the rectangular mesh for remote applied stresses of 12 and 400 MPa, respectively, while the two dash-dot curves represent results from the radial mesh at the same stress levels. Experimental results are shown by the symbols. In all cases, the lower stress level represents an elastic case and the higher stress level represents an elastic-plastic case. For this layup, the yielding of the matrix causes the slit-tip strain concentration to decrease rather than increase (as shown in Figure 6) and the analysis using the rectangular mesh predicts this trend correctly. The analytical predictions using the radial mesh incorrectly predicted that the strain concentration would increase with increasing plasticity. For both the elastic and elastic-plastic stress levels, the rectangular mesh produced predictions that were in better agreement with the experimental results in the region close to the slit tip. The elastic-plastic prediction crosses over the elastic prediction very close to the experimental data. Thus, the rectangular mesh will be used for the remainder of the analyses presented.

Figure 12 compares the analytical predictions using the rectangular mesh only to the test results for the $[0]_8$ laminate with 2a = 19 mm. The solid curve and the circular symbols represent the normalized strains for an applied stress of 12 MPa and the dashed

curve and the square symbols are for an applied stress of 400 MPa. For this layup, the analytical predictions and the experimental results are in very good agreement for both the elastic and elastic-plastic cases over the entire region.

Figure 13 compares the analytical predictions with the experimental results for the $[0/\pm45/90]_s$ layup with 2a = 19 mm. The two curves represent the analytical predictions while the symbols represent the experimental data. The results are shown for applied stress levels of 7 and 100 MPa. There is good agreement between the experimental results and the analytic predictions. Here the analysis shows that the slit-tip strain concentration factor increases with increasing plasticity, as was shown experimentally for this layup.

Figure 14 compares the analytical predictions with the experimental results for the $[0_2/\pm45]_s$ with 2a = 19 mm. The two curves represent the analytical predictions while the symbols represent the experimental data. The results are shown for applied stress levels of 11 and 200 MPa. Again, we see good agreement between the experimental results and the analytical predictions. The yielding of the matrix causes the strain concentration factor at the slit tip to increase for this layup.

The strain distributions in the $[0/90]_{2s}$ and the $[\pm45]_{2s}$ layups were also predicted but are not shown here. The $[0/90]_{2s}$ predictions were very close to the data. The analytical predictions did not agree well with the data for the $[\pm45]_{2s}$ layup. In this case the strain gages indicated higher strain levels than predicted by the analysis. However, since the load carrying plies in this laminate are at 45^o, the strain gages could not measure the strains in those

fibers. The finite element analysis could predict the fibers axial stresses and strains in the 45^{o} ply and found that the normalized strain concentration (and stress concentration) did increase with increasing plasticity. Further, the $[\pm 45]_{2s}$ layup may experience fiber rotation or extensive interlaminar yielding that the PAFAC program does not currently model, which would also result in low predictions from the analysis.

Figure 15 shows the predicted longitudinal stress in the fiber closest to the slit tip, normalized by the applied stress, for all the layups containing 0^{o} plies. The fiber stress concentration factor is shown for both an elastic and an elastic-plastic case for each layup. As previously noted, for the $[0]_{8}$ laminate, the plastic prediction is lower than the elastic prediction, while for all the other layups, the plastic predictions are higher than the elastic predictions.

IV. DISCUSSION OF RESULTS

We have shown experimentally and analytically that matrix yielding can significantly affect the fiber stress concentration. Basically two mechanisms of matrix yielding are working either to decrease the fiber stress concentration or increase it.

The first mechanism was observed in the unidirectional layup. High shear stresses in the matrix material between the slit tip and the first continuous fiber form very long yield bands (as shown in Figure 7) that tend to isolate the remaining net section from the slit thus reducing the strain concentration due to the slit. This effect, to a lesser extent, may be present in any layup containing 0^{o}

plies as shown by Post et al. (see Figure 10).

The second mechanism is present in all MMC that experience matrix yielding; when the matrix yields the load is transferred to the load carrying 0^{o} plies. The actual sequence of events is as follows: as the off-axis plies yield (and they yield before the 0^{o} plies), the load is transferred to the 0^{o} plies; as the matrix in the 0^{o} plies yields, more load goes into the 0^{o} fibers. Since for silicon-carbide/aluminum composites the matrix has approximately 20 percent as much stiffness as the fibers, when the matrix loses stiffness, considerable load is transferred to the 0^{o} fibers. The matrix is, of course, yielded more extensively closer to the slit tip. As a result, more load is transferred locally into the fibers in that region, thus, increasing the strain concentration at the slit tip.

V. CONCLUSIONS

Continuous fiber silicon-carbide/aluminum composite laminates with slits were tested statically to failure. Five different layups were examined: $[0]_8$, $[0_2/\pm45]_s$, $[0/90]_{2s}$, $[0/\pm45/90]_s$, and $[\pm45]_{2s}$. Either a 9.5 or a 19 mm slit was machined in the center of each specimen. The strain distribution ahead of the slit tip was found experimentally with a series of strain gages bonded ahead of the slit tip. A three-dimensional finite element program (PAFAC) was used to predict the strain distribution ahead of the slit tip for several layups.

For all layups, except the $[0]_8$, the yielding of the metal matrix caused the fiber stress concentration factor to increase with

increasing load. This increase is primarily due to the load being transferred out of the yielded matrix material and into the load carrying 0^{o} fibers. The finite element analysis predicted this trend correctly. This is contrary to the behavior seen in homogeneous materials where yielding causes the stress concentration to drop.

For the $[0]_8$ laminate, yielding of the matrix caused a decrease in the fiber stress concentration. This decrease was due to shear stress bands that form at the tip of the slit and grow parallel to the fibers. These shear band essentially isolate the notch effect from the remaining net section, thus lowering the strain concentration. Again, the analysis agreed with the experimental results for this layup.

APPENDIX

MATERIAL MODEL OF PAFAC PROGRAM

The model consists of an elastic-plastic matrix unidirectionally reinforced by continuous elastic fibers. Both constituents are assumed to be homogeneous and isotropic. The fibers are assumed to have a very small diameter, so that although the fibers occupy a finite volume fraction of the composite, they do not interfere with matrix deformation in the two transverse directions, but only in the axial (fiber) direction. Figure 16 shows a schematic of this lamina model. It can also be represented by parallel fiber and matrix bars or plates with axial coupling, as illustrated in Figure 16. In Figure 16, the fiber (axial) direction is parallel to the x_3-axis, and the x_1- and x_2-axes represent the transverse directions.

If the Cartesian coordinates are chosen so the x_3 coincides with the fiber direction, the second-order tensors of the independent stress and strain components, σ and ϵ, are expressed as

$$\sigma = [\sigma_{11} \ \sigma_{22} \ \sigma_{33} \ \sigma_{12} \ \sigma_{13} \ \sigma_{23}]^T$$
$$\epsilon = [\epsilon_{11} \ \epsilon_{22} \ \epsilon_{33} \ \gamma_{12} \ \gamma_{13} \ \gamma_{23}]^T$$

where $\gamma_{ij} = 2\epsilon_{ij}$ $(i, j = 1, 2, 3; i \neq j)$ are the engineering shear strain components.

For equilibrium and compatibility, several requirements are imposed on the material model shown in Figure 16. The stress average in each constituent can be related to the overall composite stress $\bar{\sigma}$ in the axial (fiber) direction as follows:

$$\bar{\sigma}_{33} = v_f(\sigma_{33})_f + v_m(\sigma_{33})_m$$

A bar over a symbol indicates overall composite stress or strain, and the subscripts f and m denote quantities related to the fiber and matrix. The volume fractions v_f and v_m are such that $v_f + v_m = 1$. The other stress components in each constituent were assumed to be uniform and to obey the following equilibrium equations:

$$\bar{\sigma}_{11} = (\sigma_{11})_f = (\sigma_{11})_m$$
$$\bar{\sigma}_{22} = (\sigma_{22})_f = (\sigma_{22})_m$$
$$\bar{\sigma}_{12} = (\sigma_{12})_f = (\sigma_{12})_m$$
$$\bar{\sigma}_{13} = (\sigma_{13})_f = (\sigma_{13})_m$$
$$\bar{\sigma}_{23} = (\sigma_{23})_f = (\sigma_{23})_m$$

The only constraint in the model is in the axial (fiber) direction; the matrix and fiber must deform equally. Thus,

$$\bar{\epsilon}_{33} = (\epsilon_{33})_f = (\epsilon_{33})_m$$

The other strain components can be related to the overall strain, $\bar{\epsilon}$ as follows:

$$\bar{\epsilon}_{ij} = v_f(\epsilon_{ij})_f + v_m(\epsilon_{ij})_m \qquad (ij \neq 33)$$

Since the fibers are elastic up to failure, the inelastic strains of the lamina are caused by matrix deformation. Because the fiber imposes an elastic constraint on the matrix which affects the shape of the lamina yield surface, additional kinematic components appear in the hardening rule of the lamina and influence the magnitude of the overall plastic strains. All aspects of the yield behavior were examined and accounted for in the formulation of the lamina

constitutive equations. These equations are explicitly described in [6,8]. The stress-strain curve of the matrix material was modeled with a Ramberg-Osgood equation [10].

REFERENCES

[1] Johnson, W. S.; Bigelow, C. A.; and Bahei-El-Din, Y. A.: Experimental and Analytical Investigation of the Fracture Processes of Boron/Aluminum Laminates Containing Notches. NASA TP-2187, National Aeronautics and Space Administration, Washington DC, 1983

[2] Poe, C. C., Jr. and Sova, J. A.: Fracture Toughness of Boron/Aluminum Laminates With Various Proportions of 0^{o} and $\pm 45^{o}$ Plies," NASA TP-1707, National Aeronautics and Space Administration, Washington DC, November 1980.

[3] Poe, C. C., Jr.: A Unifying Strain Criterion For Fracture of Fibrous Composite Laminates, Engineering Fracture Mechanics, Vol 17, No. 2, pp. 153-171, 1983.

[4] Johnson, W.S.; and Wallis, R.R.: "Fatigue Behavior of Continuous-Fiber Silicon Carbide/Aluminum Composites," Composite Materials: Fatigue and Fracture, ASTM STP 907, H.T. Hahn, Ed., American Society for Testing and Materials, Philadelphia, 1986, pp. 161-175.

[5] Goree, J.G.; and Jones, W.F.: Fracture Behavior of Unidirectional Boron/Aluminum Composite Laminates. NASA CR-3753, National Aeronautics and Space Administration, Washington DC, December, 1983.

[6] Bigelow, C. A.; and Bahei-El-Din, Y. A.: Plastic and Failure Analysis of Composites (PAFAC). LAR-13183, COSMIC, Univ. of Georgia, 1983.

[7] Bahei-El-Din, Y. A.; Dvorak, G. J.; and Utku, S.: Finite Element Analysis of Elastic-Plastic Fibrous Composite Structures. Comput. & Struct., vol. 13, no. 1-3, June 1981, pp. 321-330.

[8] Bahei-El-Din, Y. A.: Plastic Analysis of Metal-Matrix Composite Laminates. Ph.D. Disser., Duke Univ., 1979.

[9] Dvorak, G. J.; and Bahei-El-Din, Y. A.: Plasticity of Composite Laminates. Research Workshop on Mechanics of Composite Materials, Duke Univ., Oct. 1978, pp. 32-54.

[10] Bahei-El-Din, Y. A.; and Dvorak, G. J.: Plastic Yielding at a Circular Hole in a Laminated FP-Al Plate. Modern Developments in Composites Materials and Structures, J. R. Vinson, ed., American Soc. Mech. Eng., c. 1979, pp. 123-147.

[11] Post, D.; Czarnek, R.; Joh, D.; Jo, J.; and Guo, Y: Elastic-Plastic Deformation of a Metal-Matrix Composite Coupon with a Center Slot. NASA CR-178013, National Aeronautics and Space Administration, Washington DC, November, 1985.

[12] Ramberg, W.; and Osgood, W. R.: Description of Stress-Strain Curves by Three Parameters. NACA TN 902, 1943.

Table I. Composite Constituent Mechanical Properties

	SCS_2 fiber 0.14 mm diameter	6061-T0 Aluminum
Elastic modulus, GPa	340	72.5
Poisson' ratio	0.25	0.33

Table II. Failure Stresses and Calculated Elastic Moduli

Laminate	Slit length,mm	Failure Stress,MPa	E_L, GPa
$[0]_8$	9.5	793	190
	19	545	
$[0_2/\pm45]_s$	9.5	363	154
	19	258	
$[0/90]_{2s}$	9.5	269	153
	19	200	
$[0/\pm45/90]_s$	9.5	259	137
	19	200	
$[\pm45]_{2s}$	9.5	177	118
	19	88	

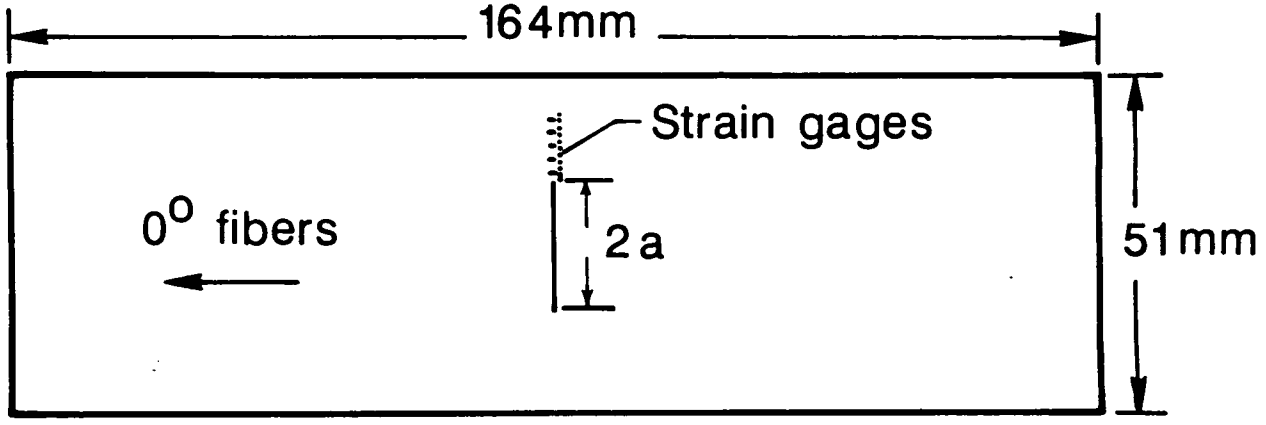

SCS-2/6061-TO ALUMINUM

$[0/\pm45/90]_{s}$ $[0_2/\pm45]_{s}$

$[0/90]_{2s}$ $[\pm45]_{2s}$

$[0]_{8}$

Figure 1. Specimen configuration.

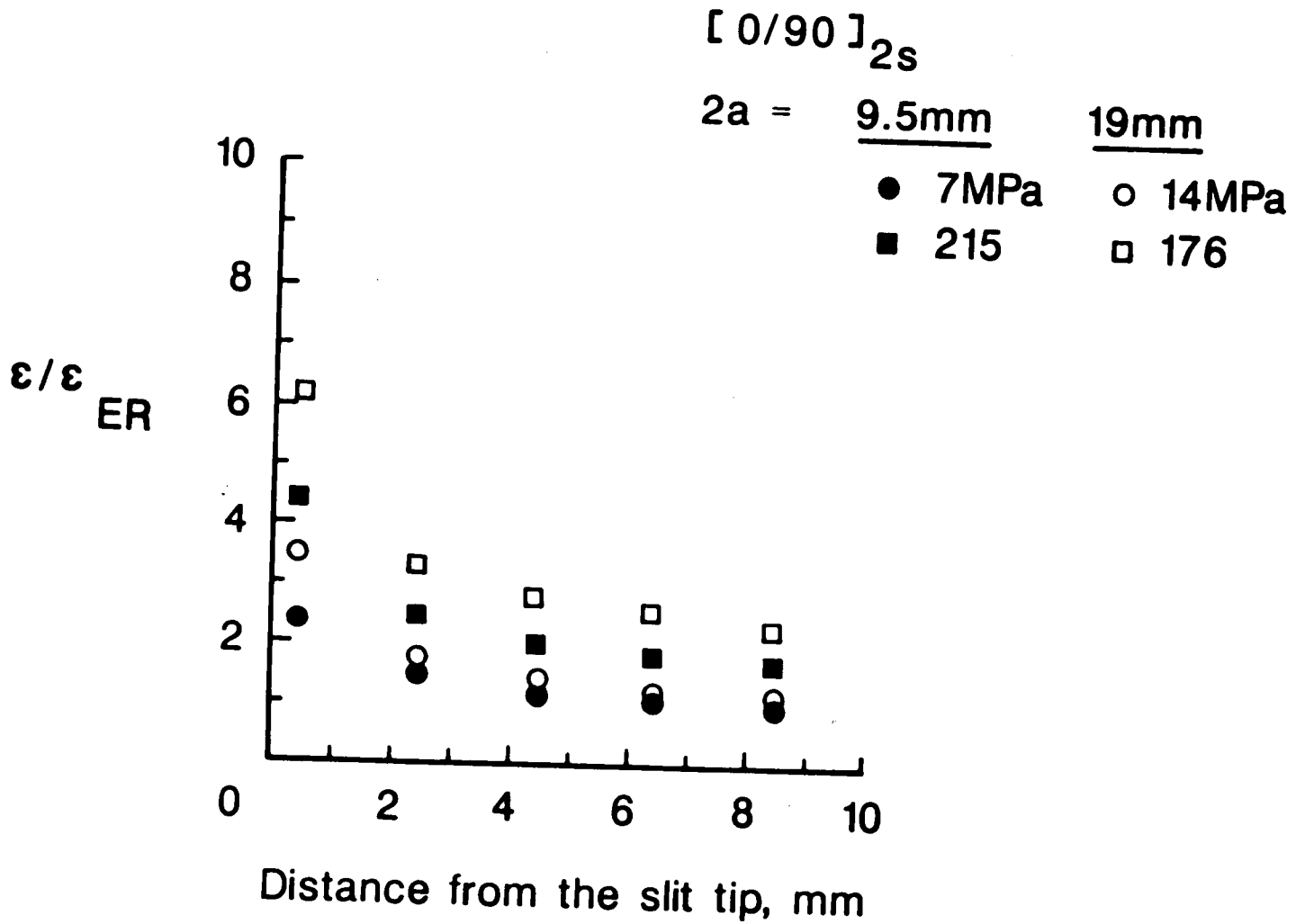

Figure 2. Normalized strain in front of slit tip for $[0/90]_{2s}$ layup.

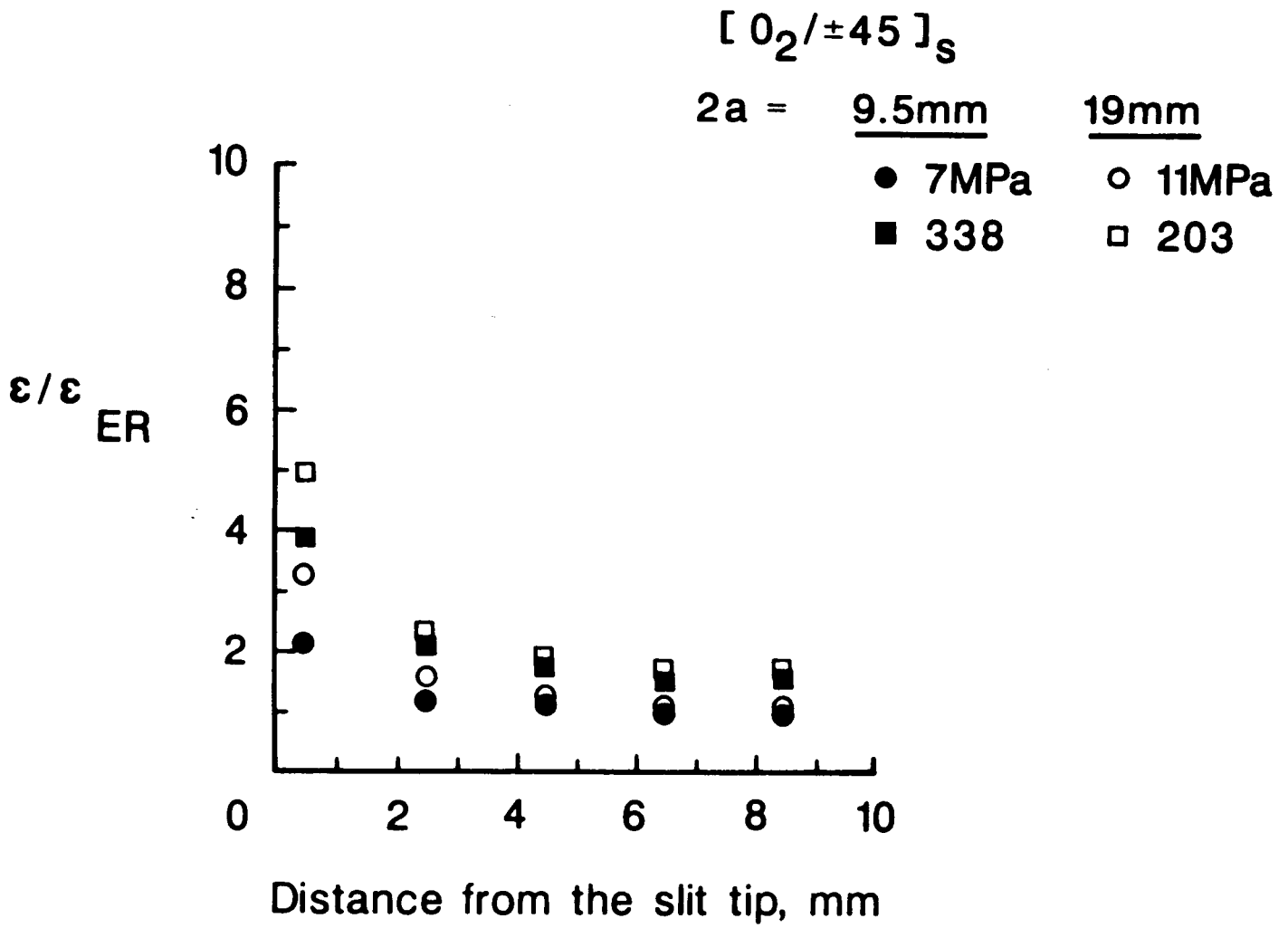

Figure 3. Normalized strain in front of slit tip for $[0_2/\pm45]_s$ layup.

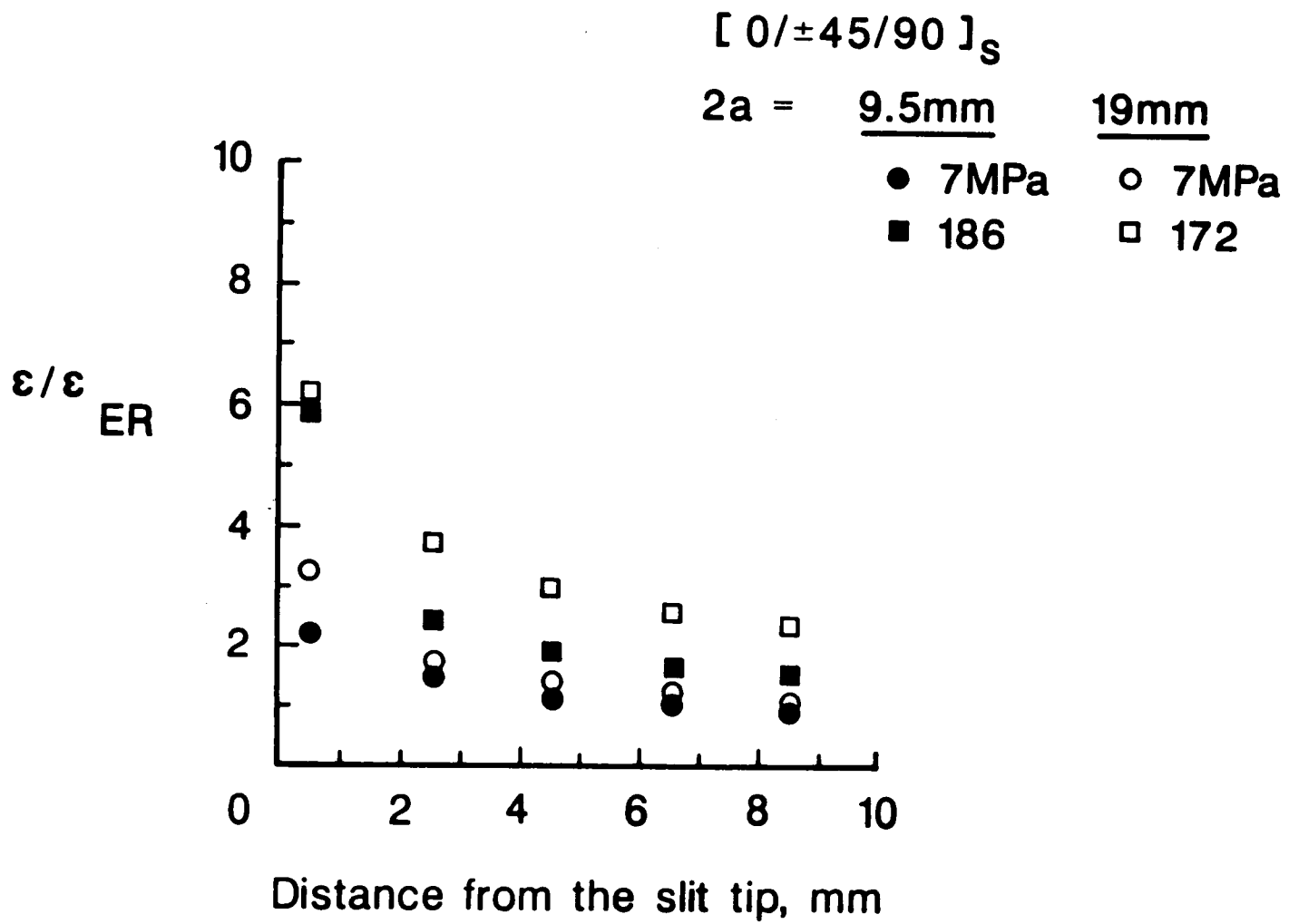

Figure 4. Normalized strain in front of slit tip for $[0/\pm45/90]_s$ layup.

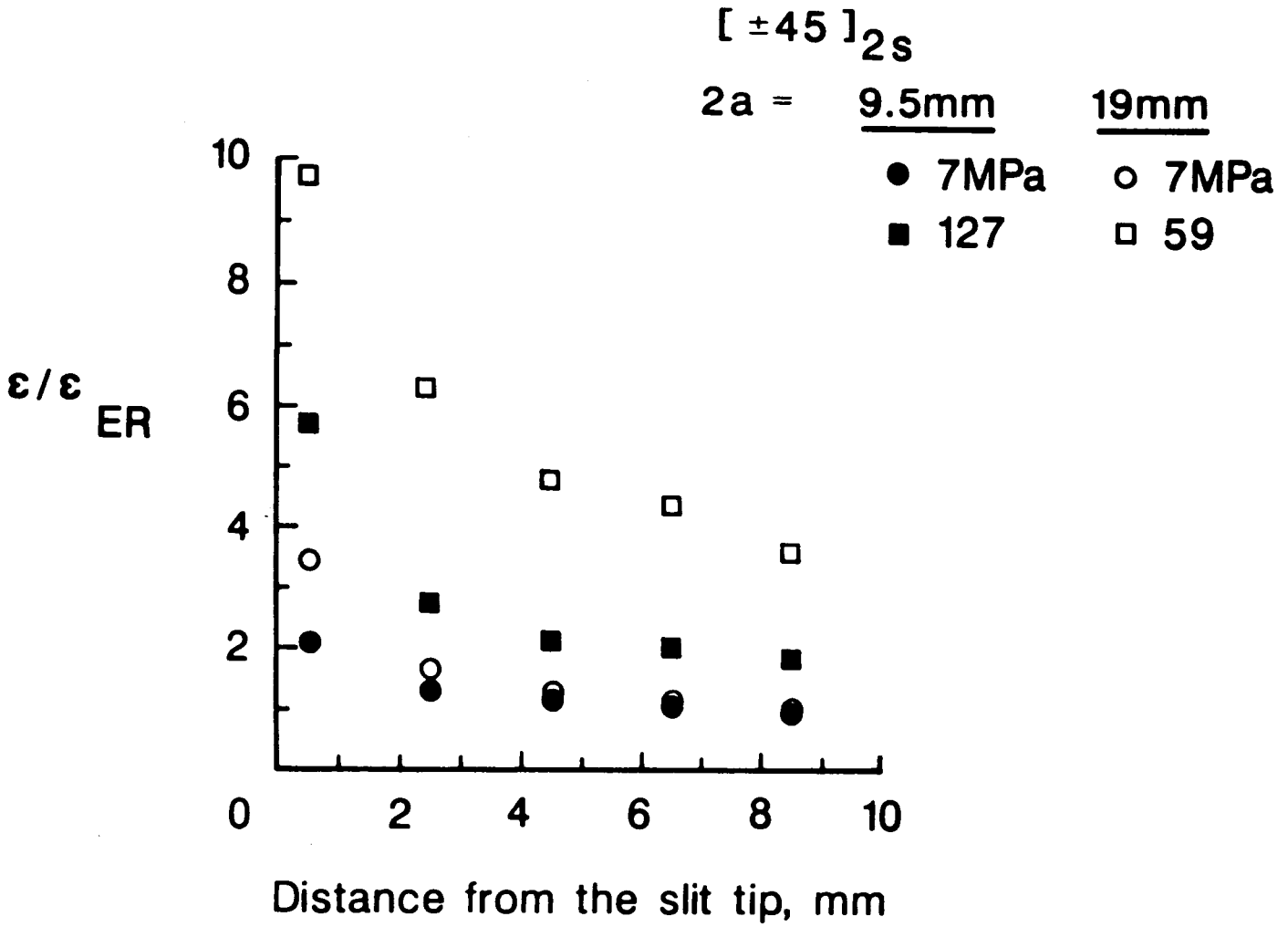

Figure 5. Normalized strain in front of slit tip for $[\pm 45]_{2s}$ layup.

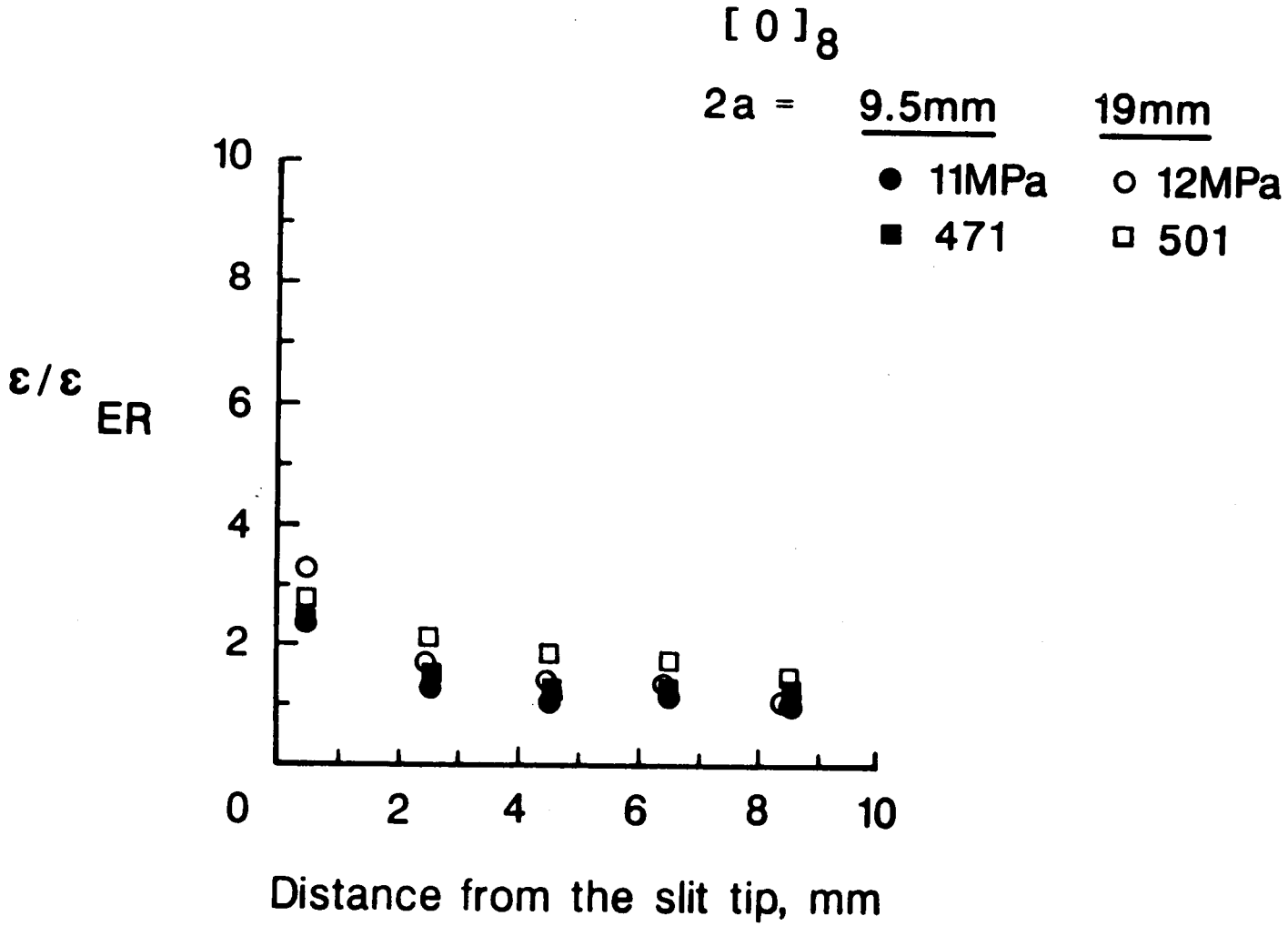

Figure 6. Normalized strain in front of slit tip for $[0]_s$ layup.

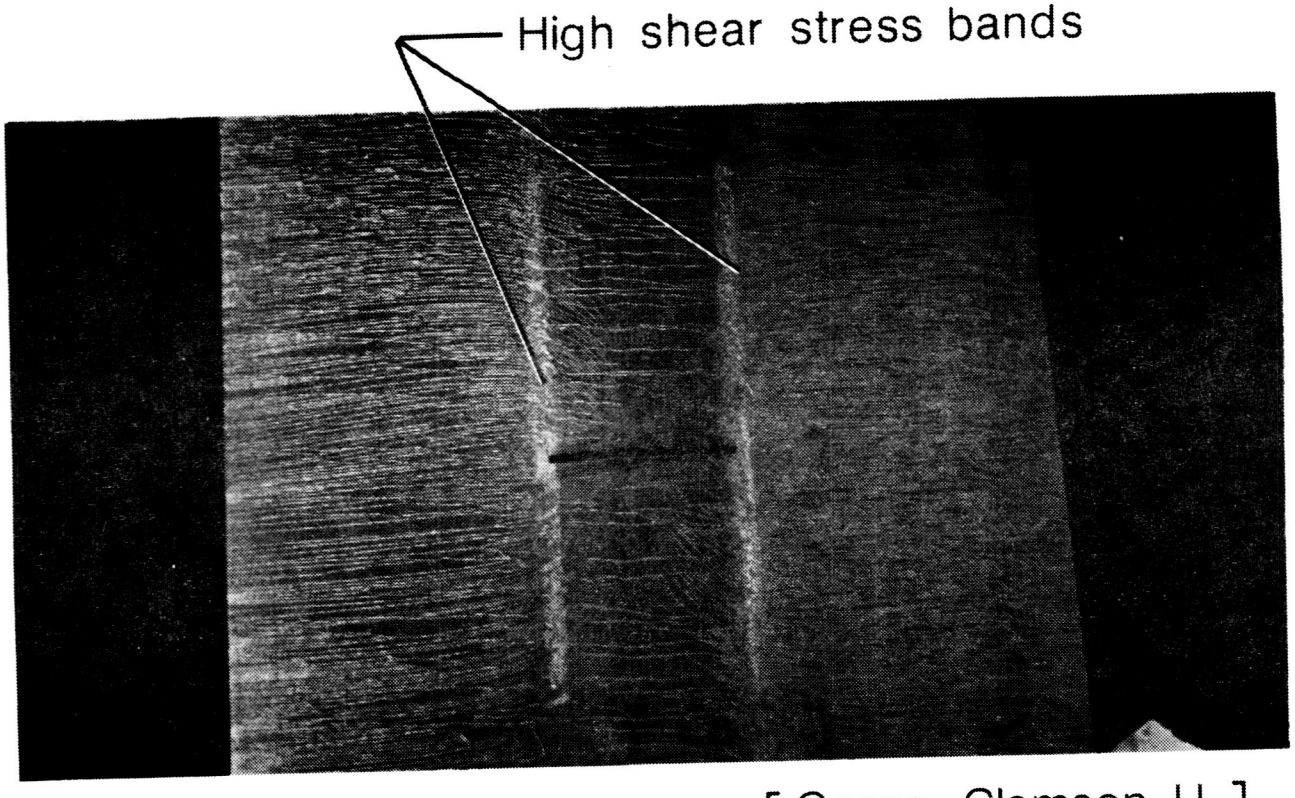

Figure 7. Brittle lacquer crack pattern at 12,500 N[3].

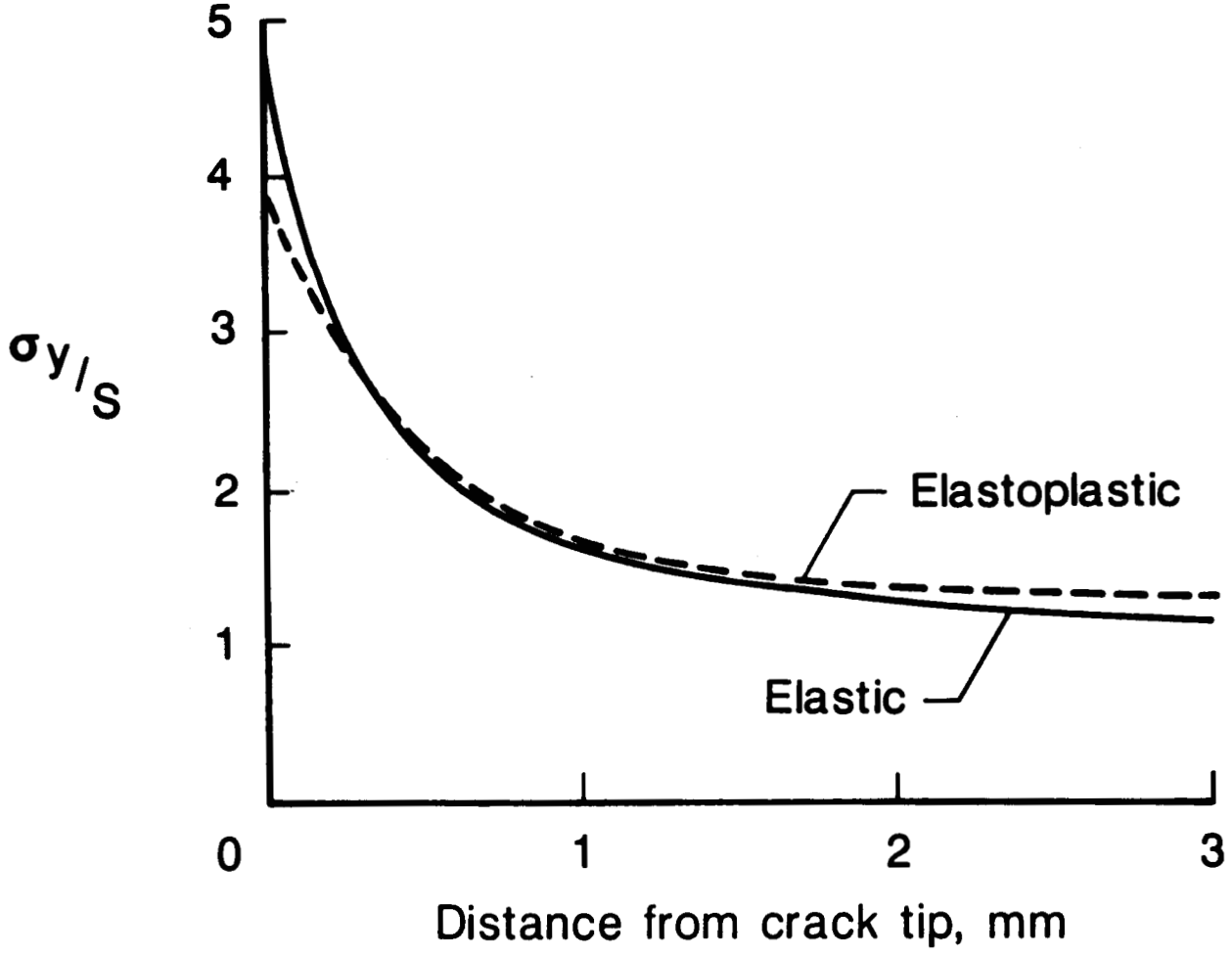

Figure 8. Stress distribution ahead of slit tip in homogeneous aluminum. 2a = 5.86 mm.

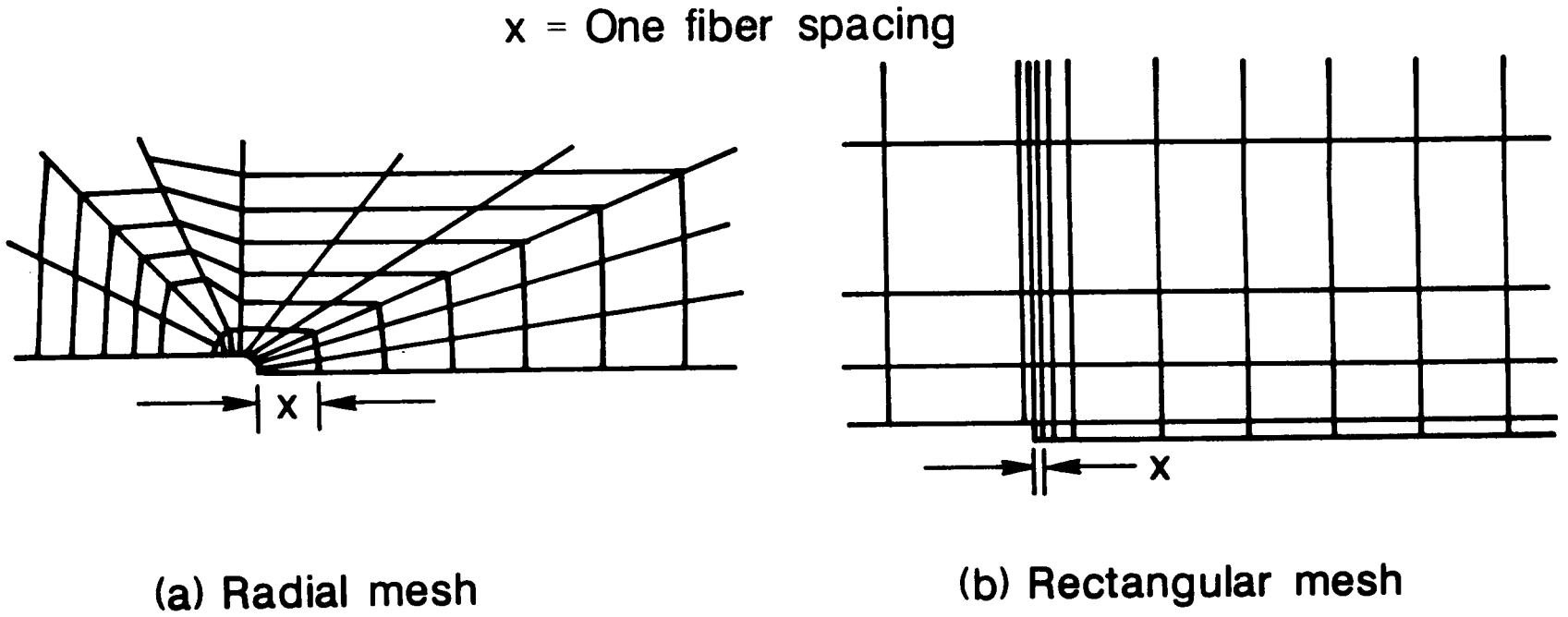

Figure 9. Finite element meshes.

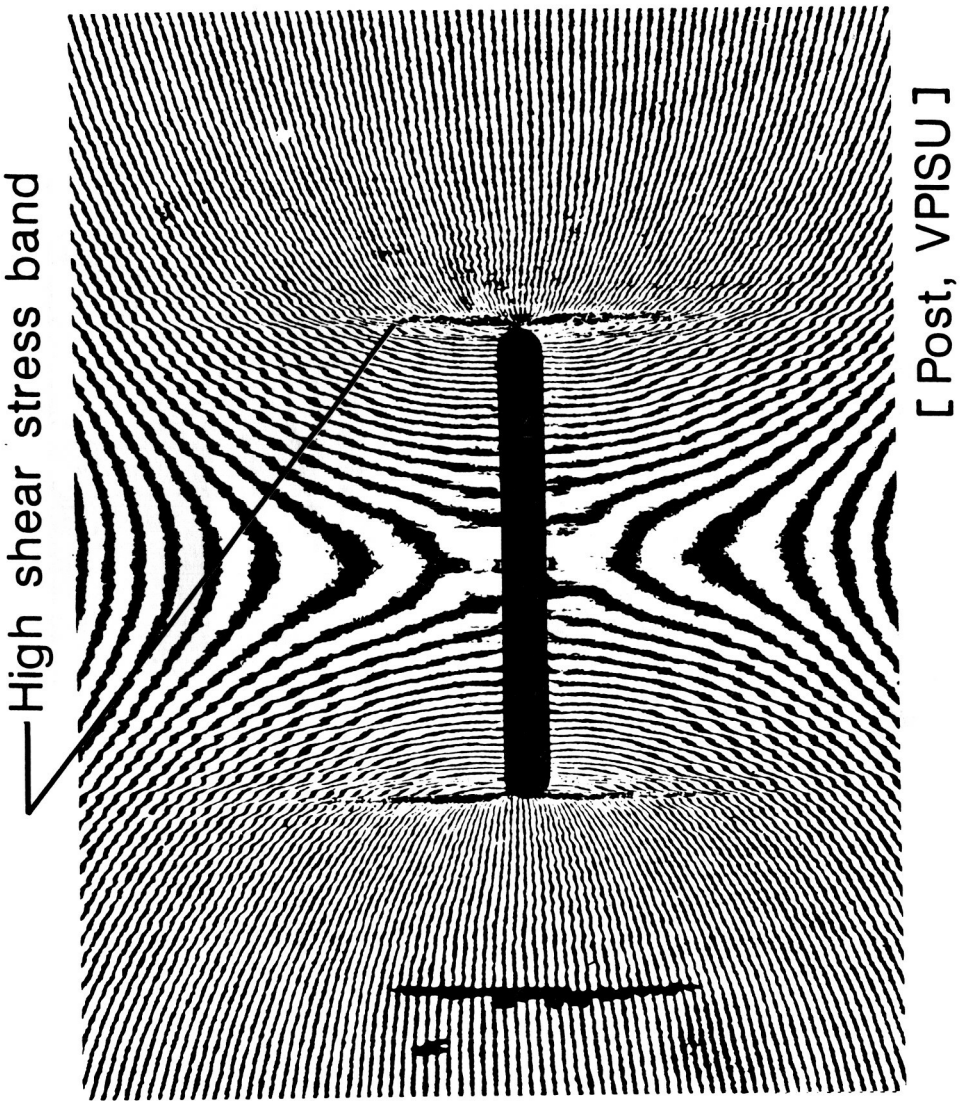

Figure 10. Moire fringes in a $[0/\pm45]_S$ boron/aluminum laminate [9].

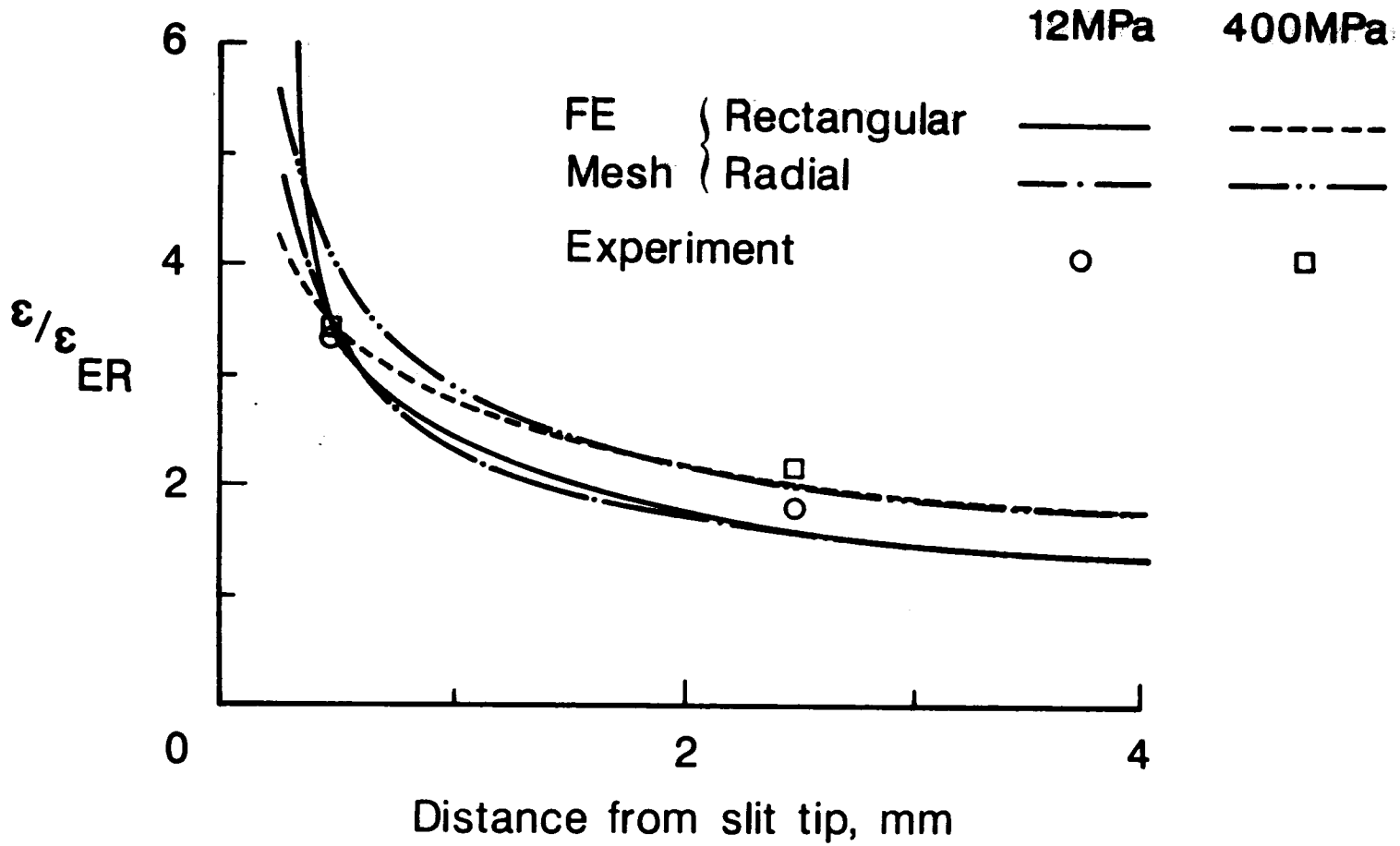

Figure 11. Comparison of rectangular and radial mesh results for $[0]_8$ layup. 2a = 19 mm.

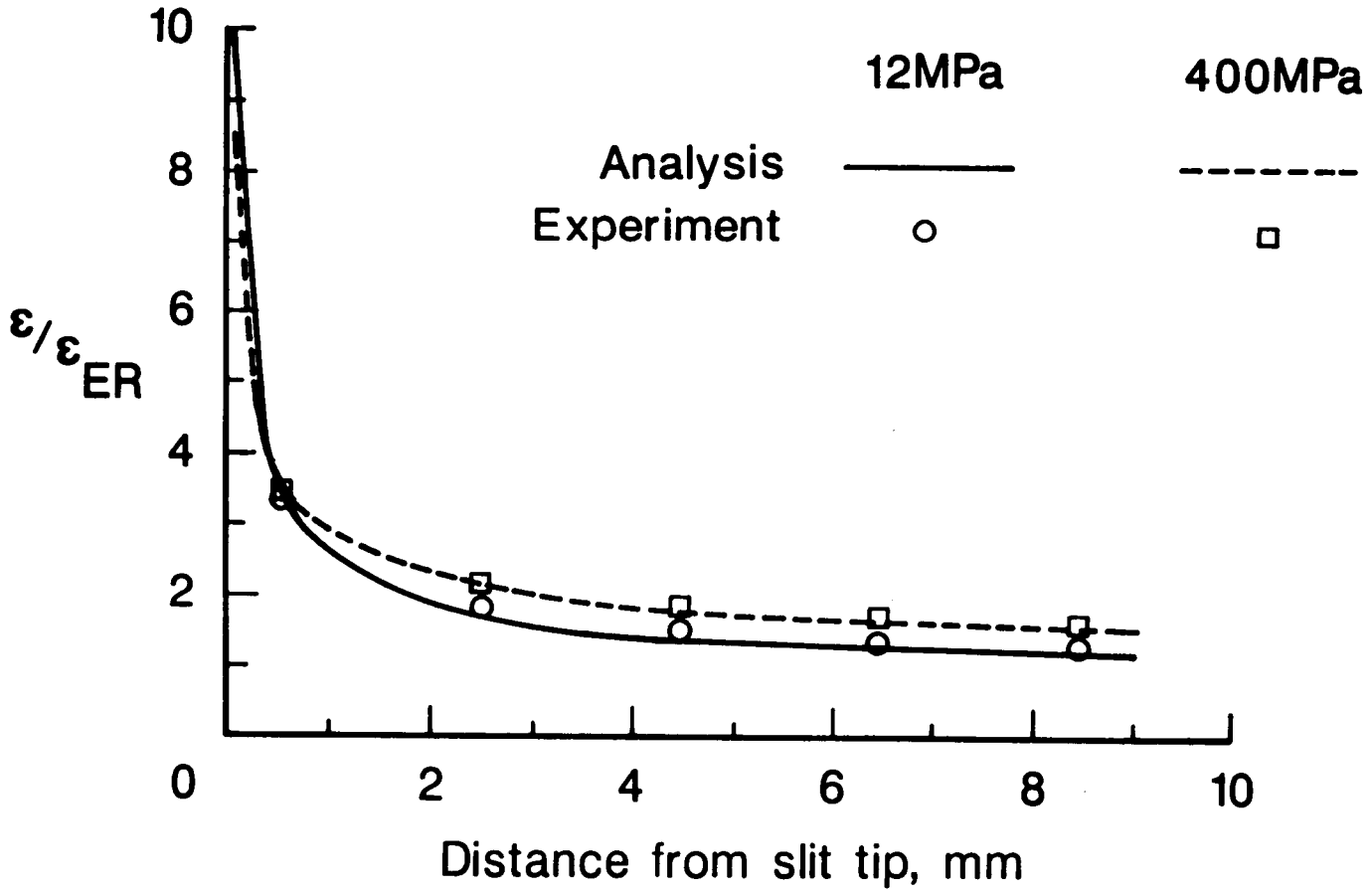

Figure 12. Normalized strain in front of slit tip with rectangular mesh for $[0]_8$ layup.

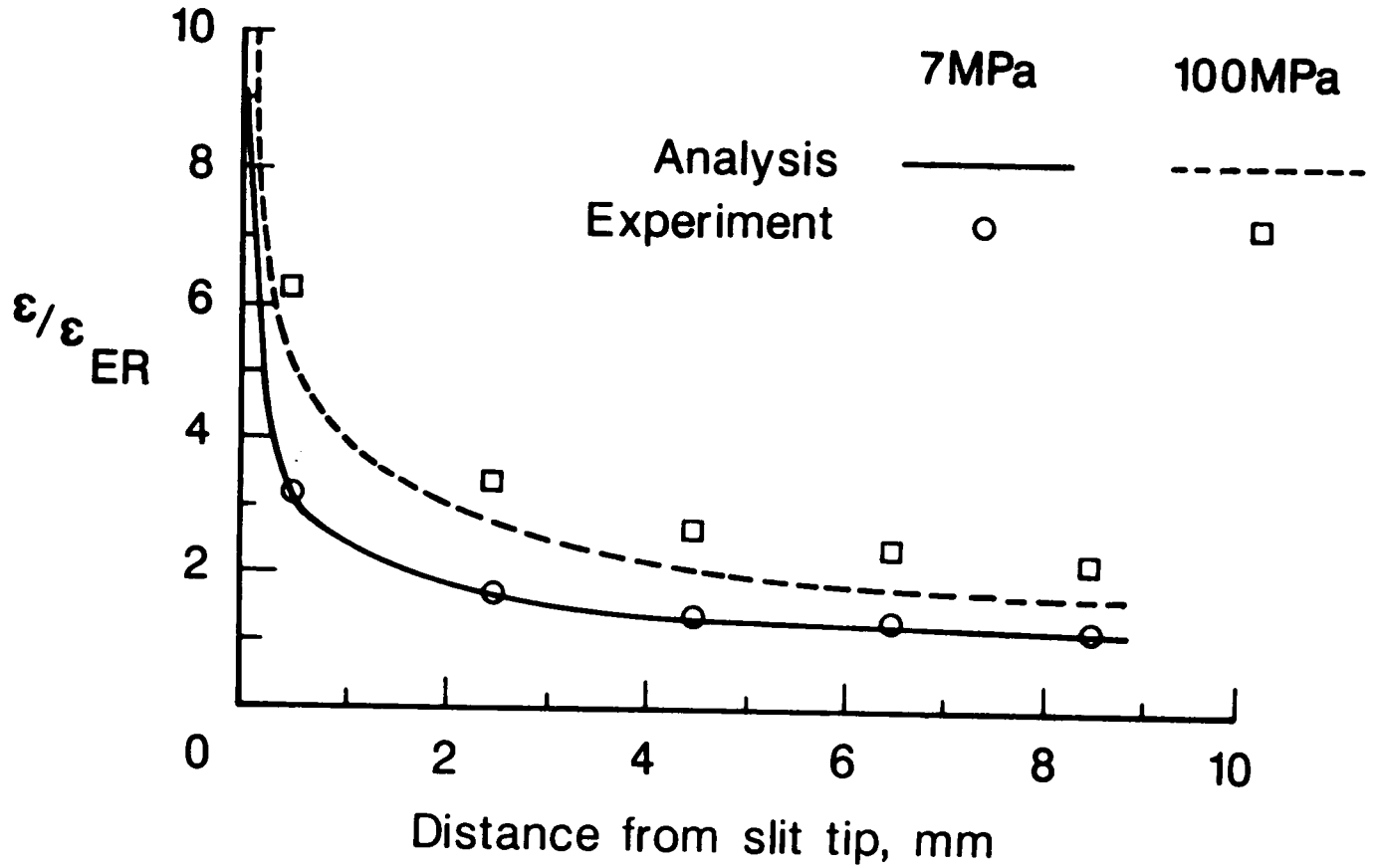

Figure 13. Normalized strain in front of slit tip with rectangular mesh for $[0/\pm45/90]_s$. 2 a = 19 mm.

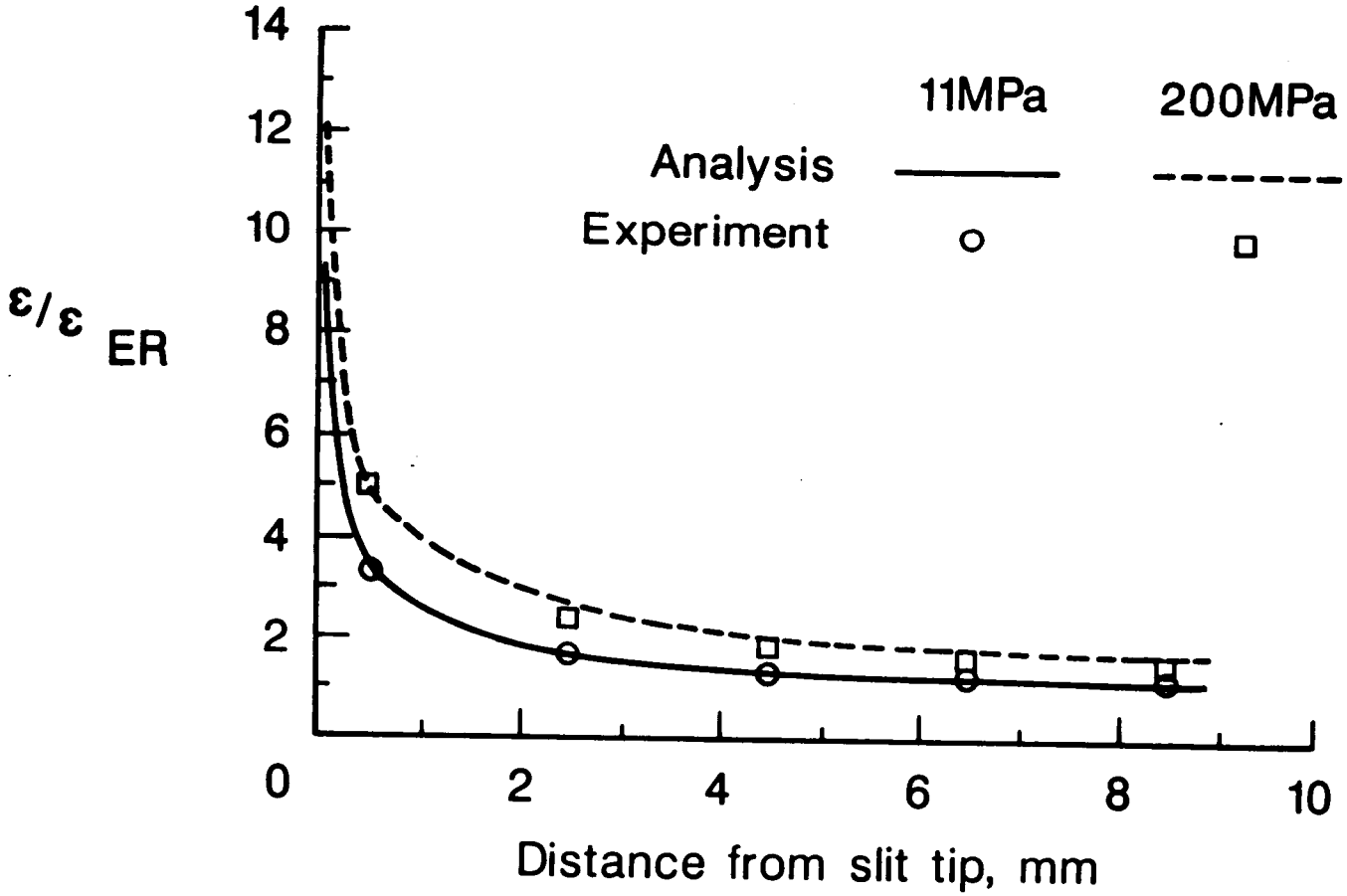

Figure 14. Normalized strain in front of slit tip with rectangular mesh for $[0_2/\pm45]_s$ layup. 2a = 19 mm.

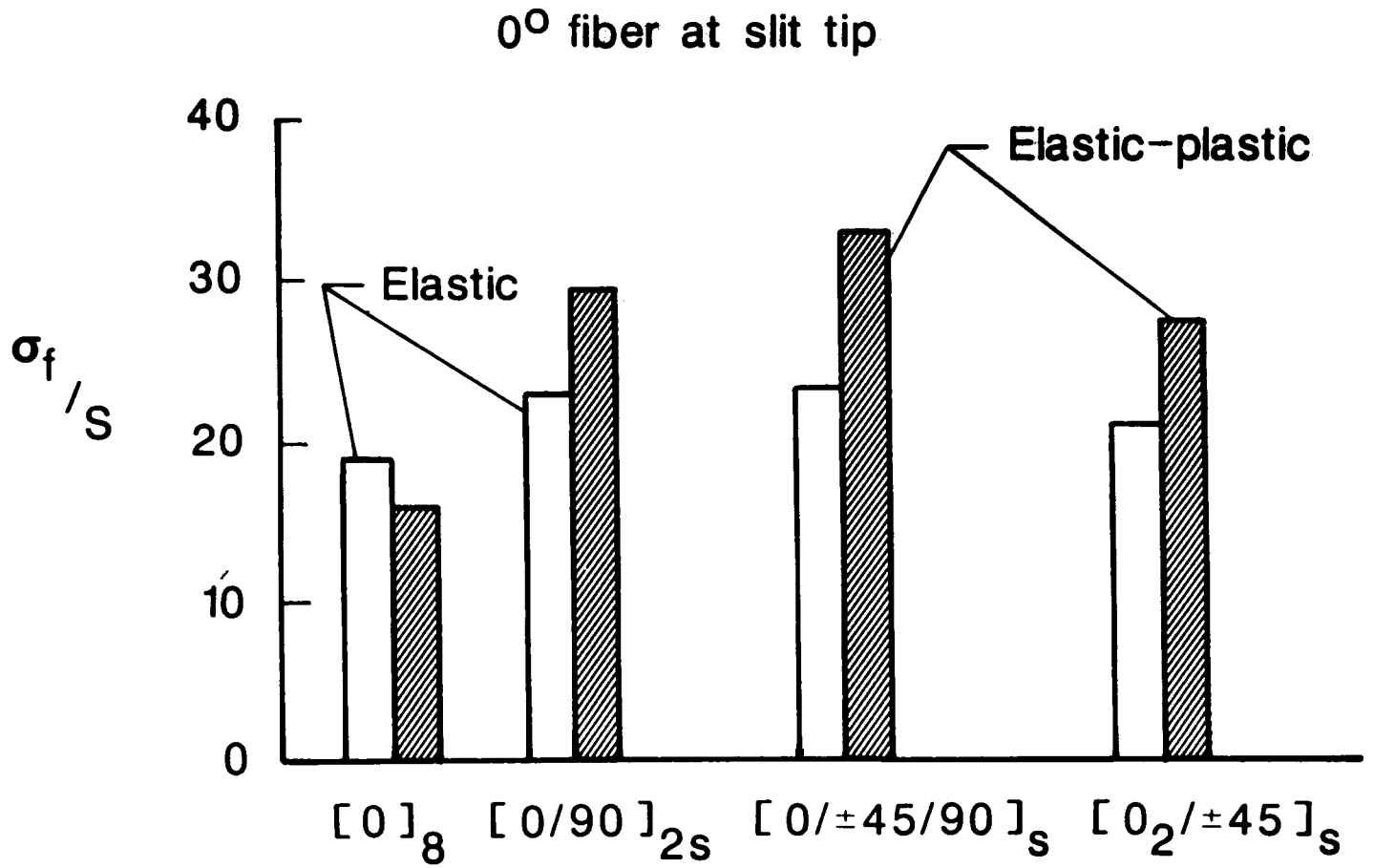

Figure 15. Fiber stress concentrations for layups containing 0°plies. 2a = 19 mm.

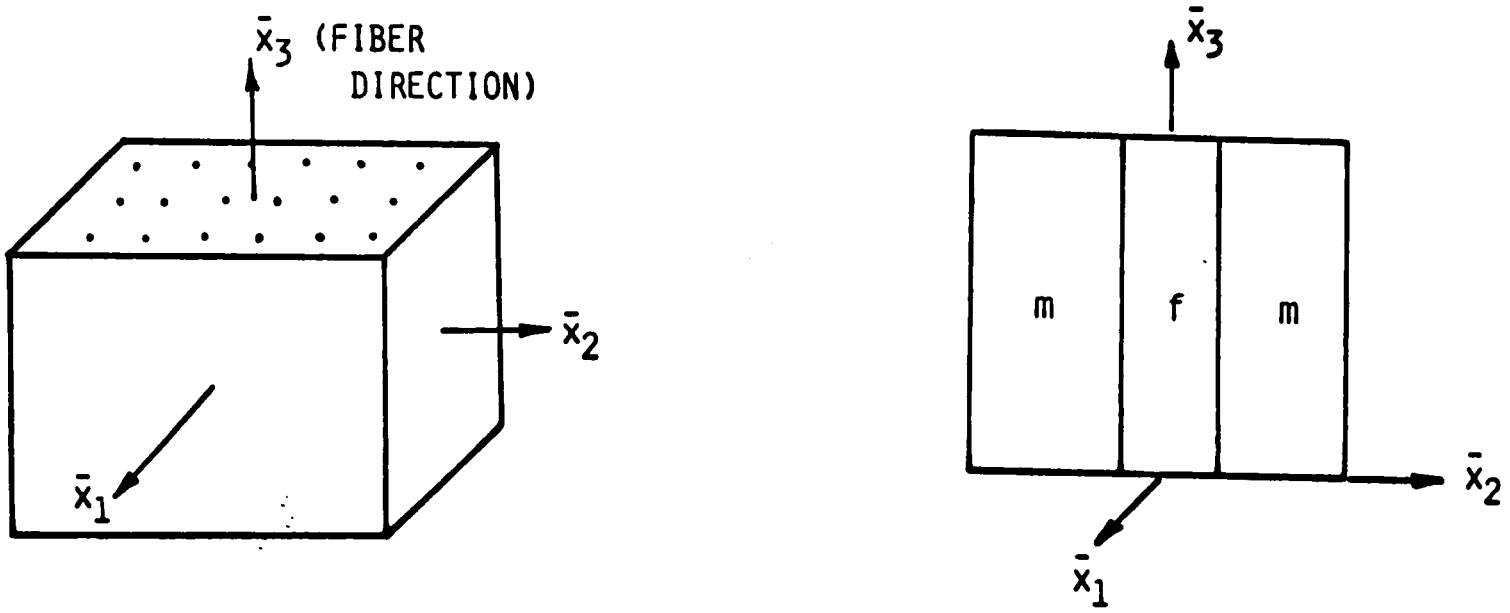

Figure 16. Element material model.

Standard Bibliographic Page

1. Report No.	2. Government Accession No.	3. Recipient's Catalog No.
NASA TM-89093		

4. Title and Subtitle	5. Report Date
ELASTIC-PLASTIC STRESS CONCENTRATIONS AROUND CRACK-LIKE NOTCHES IN CONTINUOUS FIBER REINFORCED METAL MATRIX COMPOSITES	February 1987
	6. Performing Organization Code: 505-63-01
7. Author(s): W. S. Johnson and C. A. Bigelow	8. Performing Organization Report No.
9. Performing Organization Name and Address: NASA Langley Research Center, Hampton, VA 23665-5225	10. Work Unit No.
	11. Contract or Grant No.
12. Sponsoring Agency Name and Address: National Aeronautics and Space Administration, Washington, DC 20546	13. Type of Report and Period Covered: Technical Memorandum
	14. Sponsoring Agency Code

15. Supplementary Notes

This paper will also be published as an ASTM STP entitled "Test Methods and Design Allowable for Fiber Composites: Second Symposium."

16. Abstract

Continuous fiber silicon-carbide/aluminum composite laminates with slits were tested statically to failure. Five different layups were examined: $[0]_8$, $[0_2/\pm45]_S$, $[0/90]_{2S}$, $[0/\pm45/90]_S$, and $[\pm45]_{2S}$. Either a 9.5 or a 19 mm slit was machined in the center of each specimen. The strain distribution ahead of the slit tip was found experimentally with a series of strain gages bonded ahead of the slit tip. A three-dimensional finite element program (PAFAC) was used to predict the strain distribution ahead of the slit tip for several layups. For all layups, except the $[0]_8$, the yielding of the metal matrix caused the fiber stress concentration factor to increase with increasing load. This is contrary to the behavior seen in homogeneous materials where yielding causes the stress concentration to drop. For the $[0]_8$ laminate, yielding of the matrix caused a decrease in the fiber stress concentration. The finite element analysis predicted these trends correctly.

17. Key Words (Suggested by Authors(s))	18. Distribution Statement
Metal matrix composites Yielding Stress concentrations Three-dimensional analysis Silicon-carbide fibers	Unclassified - Unlimited Subject Category - 24

19. Security Classif.(of this report)	20. Security Classif.(of this page)	21. No. of Pages	22. Price
Unclassified	Unclassified	36	A03

For sale by the National Technical Information Service, Springfield, Virginia 22161